

Entanglement Entropy Coarse-Graining, Surfaces of Ignorance, and the Foundations of Quantum Statistical Mechanics

Shannon Ray,^{1,2} Paul M. Alsing,¹ Carlo Cafaro,³ and H S. Jacinto¹

¹*Information Directorate, Air Force Research Laboratory, Rome, NY 13441, USA*

²*Griffiss Institute, Rome, NY 13441, USA*

³*Department of Mathematics and Physics, SUNY Polytechnic Institute, 12203 Albany, New York, USA*

It has been established that the entanglement entropy functions as a thermal entropy for closed many-body systems. In this work, we introduce the entanglement coarse-graining (ECG) which is a quantum coarse-graining defined for the entanglement entropy. For the examples considered, we show that it reproduces two key features of the original Boltzmann coarse-graining (BCG). These are the relationship between volume of macro-states, order, and equilibrium and that the vast majority of the state space consists of the equilibrium macro-state. The equilibrium macro-state is characterized by maximum entanglement. We show that the volume behaves like the von Neumann entropy of the subsystem ρ_S derived from the pure composite system $|\psi_{ES}\rangle$ in that both are zero for pure states, maximal for maximally mixed states, and concave functions w.r.t the purity of ρ_S . This implies that the volume of each macro-state represents the missing information in ρ_S due to its entanglement with the environment. For this reason, we call the macro-states surfaces of ignorance. Each macro-state is constructed using the Lie group symmetries underlying the Hilbert space in which the system is defined. Because of this, each macro-state is also a differential manifold. Volumes are computed directly from the metric components which are defined in this work. We present examples for systems whose symmetries are defined by $SO(3)$, $SU(2)$, and $SO(N)$. The ECG is also unique in that it reproduces features of typicality that are characteristic of the BCG without assuming the dimension of $|\psi_{ES}\rangle$ to be large. Also, the relationship between equilibrium and maximum entanglement may give new meaning to the well-known fact that most pure states of composite systems are maximally entangled in terms of thermalization, equilibrium, and the second law of thermodynamics.

I. INTRODUCTION

A. Boltzmann Coarse-Graining

In 1872, Boltzmann attempted to prove his H -theorem which he hoped would give a theoretical foundation for the second law of thermodynamics [1]. The goal was to show that for a closed system consisting of a gas of M particles with total energy E isolated within a volume V , there existed a quantity H that only evolved monotonically regardless of the initial distribution of the gas in the 6-dimensional single particle phase space known as μ -space. The evolution of the system was modeled by treating each gas molecule as hard spheres that evolved under Hamilton's equations. Additional constraints on the density of gas were assumed to guarantee the correct circumstances for frequent binary collisions only. Boltzmann's H -theorem received criticism upon arrival. This criticism led to the Boltzmann coarse-graining (BCG) and entropy which are foundational to statistical mechanics.

One criticism was the problem of the reversibility of Hamilton's equations proposed by Loschmidt. Loschmidt's paradox asks the question, how could H be strictly increasing regardless of the initial state of the gas if it is possible to use as one's initial state the end result of a diffusion process with the momenta of all particles reversed? Since Hamilton's equations are reversible, the gas should collapse back to the initial state of the diffusion process which is more ordered. Boltzmann

responded to this criticism by introducing his coarse-graining (CG) of the $6N$ -dimensional phase space, known as γ -space, to argue that the likelihood of such states being observed is vanishingly small. The purpose of this paper is to introduce the entanglement coarse-graining (ECG), which is a quantum analogue of the BCG associated with the entanglement entropy for closed many-body systems. It is not the goal of this paper to develop a quantum H -theorem, and we do not define a quantum Boltzmann entropy with the ECG. We merely examine volumes of the macro-states. Defining a proper entropy is left for future research.

The main element of Boltzmann's argument was the use of combinatorics to count all of the ways the gas could be equivalently distributed in μ -space. This results in a demarcation of γ -space into disjoint sets (see Fig. 1) called macro-states where each distribution on μ -space coincides with a unique macro-state. Each macro-state has many micro-state representations since the particles are indistinguishable and can be interchanged without changing the results of any measurement on the system. The number of micro-states associated with a macro-state is defined as the multiplicity. Given this CG, Boltzmann argued that macro-states with greater multiplicity are more likely to be observed than those with less multiplicity since there are more equivalent ways for the system to be arranged with that distribution. In fact, the volume of γ -space consisting of a macro-state is proportional to its multiplicity. This relationship between multiplicity and volume provides an interpretation of the

probability of observing a macro-state in terms of its volume in γ -space. This made Boltzmann's rebuttal an argument of typicality. Even if a system begins out of equilibrium in an atypical macro-state, those macro-states take up vanishingly small volumes of γ -space and the system will quickly evolve to macro-states with successively larger volumes until it reaches the equilibrium macro-state, which is the most typical and takes up the vast majority of γ -space.

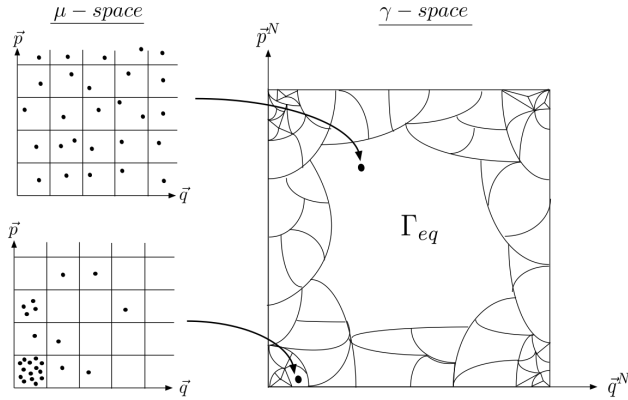


FIG. 1. Illustration of Boltzmann's original approach to coarse-graining inspired by figure 2 in [2]. On the left are examples of distributions on μ -space, while the right depicts the coarse-graining of γ -space. By dividing μ -space into equal cells, macro-states are defined by simply counting the number of particles in each cell. Since each particle is indistinguishable, interchanging which particle occupies each cell does not change the macro-state; thus, there are many equivalent micro-states for each macro-state. The size of each macro-state depends on the number of micro-states it has. Boltzmann showed that distributions on μ -space that are more uniform have more micro-states, and the largest macro-state, Γ_{eq} , is associated with a gas in equilibrium.

Ultimately, it is not clear whether or not Boltzmann was successful in his endeavor. The meaning of his H -theorem is fraught with controversy [3], and it is not clear how he justified the probabilistic interpretation of his CG without the use of something like the ergodic hypothesis [1]. Despite these controversies, the BCG and entropy are foundational to statistical mechanics due to how well their probabilistic interpretations agree with observation. They also give insight into the problem of reversibility of closed systems, the process of thermalization, and what it means for a system to be in equilibrium using arguments of typicality [4, 5]. The extension of these insights in regard to quantum entanglement of closed systems is an important property of the ECG.

Typicality arguments regarding reversibility, thermalization, and equilibrium rely on two key features of the BCG. The first key feature is the relationship between volume, order, and equilibrium. In Boltzmann's formalism, macro-states that are more ordered have fewer micro-states and are consistent with distributions on

μ -space that are less uniform. Macro-states that are more disordered have more micro-states and are consistent with distributions on μ -space that are more uniform. Therefore, thermalization is understood as a system evolving from less uniform distributions to more uniform distributions through a trajectory of macro-states with less volume to those with greater volume [6, 7]. Eventually, the system reaches equilibrium, which is the most typical macro-state with the largest volume. This leads to the second key feature of the BCG which is that the vast majority of γ -space consists of the equilibrium macro-state. The fraction of γ -space consisting of the equilibrium macro-state grows as the number of particles increase, and for systems where the number of degrees of freedom are on the order of Avogadro's number, the equilibrium macro-state makes up over 99.99% (as a representative value) of the space [2, 8–10]. A major goal of this paper is to provide evidence that the ECG captures these two key features of the BCG.

B. Relevant Background and Contributions

During the evolution of a pure closed state $|\psi_{ES}\rangle$, the von Neumann entropy, S_{VN} , maintains a constant value of zero. This leaves the problem of determining which thermodynamic entropy quantifies the system's evolution from more ordered states to a less ordered state? It has been established [11–14] that the entanglement entropy functions as a local measure of thermal entropy. The entanglement entropy between S and E is defined as the von Neumann entropy of $\rho_S = \text{Tr}_E[|\psi_{ES}\rangle\langle\psi_{ES}|]$ or $\rho_E = \text{Tr}_S[|\psi_{ES}\rangle\langle\psi_{ES}|]$ since they are equivalent due to the Schmidt decomposition. Given this definition of quantum thermal entropy, states where ρ_S and ρ_E are more separable are more ordered, and states where ρ_S and ρ_E are less separable are less ordered. Despite the success of the entanglement entropy in defining a quantum thermal entropy, there has yet to be a well-defined coarse-graining associated with it, until now.

The macro-states of the ECG are defined as the set of purifications $F^{\rho_S} \equiv \{|\bar{\Gamma}_{ES}^{\rho_S}\rangle\} \subset \mathcal{H}_{ES} \equiv \mathcal{H}_E \otimes \mathcal{H}_S$ of ρ_S , and micro-states are elements of F^{ρ_S} ; since there is a 1-to-1 correspondence between F^{ρ_S} and ρ_S , ρ_S 's are also understood as the macro-states. This demarcates \mathcal{H}_{ES} into disjoint sets where each macro-state and its volume are uniquely associated with an entanglement entropy. And since the entanglement entropy is a thermal entropy, each macro-state coincides with a unique thermal entropy.

There are many approaches to characterizing thermalization and equilibrium for closed quantum systems [2, 10, 15–27]. Some focus on more realistic systems with specific Hamiltonians and initial conditions for thermalization [17, 21, 23]. Our analysis is less interested in specific systems and evolutions, and is only concerned with thermalization as it relates to entanglement between subsystems of the total system. This places our analysis

inline with those in [20, 22] which are more generic.

In [20], the authors keep their analysis very generic with the only restrictions being that total system $|\psi_{ES}\rangle$ is decomposed into system S and environment E such that $\dim(S) \ll \dim(E)$, the number of degrees of freedom of $|\psi_{ES}\rangle$ is large, and there exists some constraint \mathcal{R} that identifies the set of possible pure states of the composite system. Typicality arguments rely on the restrictions that $|\psi_{ES}\rangle$ is large and $\dim(S) \ll \dim(E)$. These restrictions are not necessary for the ECG. The analysis in [20] is made more specific in [22], though it is still very generic, by considering dynamics associated with non-degenerate Hamiltonians with many eigenstates such that S and E must interact. In both cases, the authors conclude that a subsystem satisfying $\dim(S) \ll \dim(E)$ will quickly equilibrate and thus the composite system will be thermalized. They argue that this might explain entanglement's role in understanding the 2nd law of thermodynamics.

Our analysis is more generic than that found in [20], but is similar in that both do not assume any specific temporal evolution of $|\psi_{ES}\rangle$ thus making our findings kinematic rather than dynamical. It also differs in that we do not assume the dimension of $|\psi_{ES}\rangle$ to be large or that $\dim(S) \ll \dim(E)$ to satisfy typicality arguments. Without these restrictions, we still provide evidence that the ECG demonstrates the typical behaviors captured by the two key features of the BCG for composite systems of low and high dimensions. The capacity to reproduce traits of typicality at low dimension seems to be unique to the ECG. We also do not assume any restriction \mathcal{R} . Instead, the ECG is a CG of the entirety of \mathcal{H}_{ES} . The only restrictions are that $|\psi_{ES}\rangle$ is pure and closed, and $\dim(S) \leq \dim(E)$. This lack of a restriction places our work in contrast with most approaches found in the literature where a micro-canonical energy shell, $E + \delta E$, or some other restriction identifies the set of accessible pure states. The ECG is a generic unique structure (given a density operator ρ_S) that underlies composite Hilbert spaces. As such, its applicability is quite broad and it may give new insights into pre-existing studies of composite systems.

To show that the ECG captures the first key feature of the BCG, we must show that $|\psi_{ES}\rangle$ would strictly evolve from F^{ρ_S} with less volume to F^{ρ_S} with greater volume in the scenario that ρ_S strictly evolves from states of lower von Neumann entropy to higher von Neumann entropy. Such an evolution is one where ρ_S and ρ_E become strictly more entangled. To demonstrate this using a kinematic approach provided by CG, it is sufficient to show that \mathcal{H}_{ES} is demarcated into a landscape of F^{ρ_S} 's where the volumes behave like S_{VN} in that they are zero on pure states, maximal on maximally mixed states and are concave functions w.r.t the purity of ρ_S . In fact, we show that the volume is an upper bound of S_{VN} for the examples considered. This relationship between volume and S_{VN} means that a unique S_{VN} is associated with each macro-state F^{ρ_S} . This is how the connection between

the ECG and the entanglement entropy is justified.

To show that the ECG captures the second key feature of the BCG, we must show that the vast majority of \mathcal{H}_{ES} consists of the equilibrium macro-state. In studies of thermalization that use arguments of typicality [10, 19, 24], this feature defines the equilibrium macro-state. This also defines the equilibrium macro-state for the ECG, but it has the additional trait that its micro-states have maximal entanglement between S and E . This may provide an alternative interpretation in terms of typicality, thermalization, and equilibrium of the well-known fact that most pure states of composite systems are maximally entangled [28]. In Sec. III, we will show that the second trait holds for composite systems consisting of two qubits and becomes more pronounced as the dimension becomes large. It is easy to see conceptually how maximum entanglement and volume corresponds to the classical notion of equilibrium using the example of adding cream to a cup of coffee.

Considering the diffusion of cream into coffee, the longer the cream and coffee interact, the more difficult it is to separate them and the more disordered the total system becomes. One would not expect the cream to spontaneously separate from the coffee assuming the system is closed. This is a classic example of the arrow of time associated with the second law of thermodynamics. Analogously, treating ρ_S and ρ_E as the cream and coffee respectively, the ECG suggests that as a closed quantum system becomes more entangled, one should not expect a pure product state $\rho_S \otimes \rho_E$ to spontaneously emerge and become stable (i.e. persist). Instead, one would expect the system to reach an equilibrium in which it remains in a maximally disordered state barring outside intervention. Thus, since equilibrium is also associated with an unchanging state of the total system [25], it is reasonable to accept the interpretation that maximum entanglement implies equilibrium.

Another feature that sets the ECG apart from other quantum CGs is the fact that the macro-states are generated using the unitaries associated with the Lie group symmetries underlying the Hilbert space in which the system is defined. Because of this, the macro-states of the ECG are also differential manifolds. This is in contrast to quantum CGs that use the von Neumann projector formalism [2, 24, 26, 27, 29] which demarcates the space of pure states into disjoint sets of orthogonal subspaces using projectors associated with observable quantities. The volume of the macro-state is then defined as the dimension spanned by the basis of each subspace. In our analysis, the ECG is defined independent of observations, and the macro-states are defined w.r.t a metric tensor which we use to compute volume. As far as we know, the ECG is the only quantum CG whose macro-state volumes are computed from a metric tensor.

The volumes of the macro-states are directly related to the missing information in ρ_S due to its entanglement to ρ_E . This implies that the more information missing from ρ_S , the more purifications there are that could complete

the missing information in ρ_S , and the more ignorant one is about the actual state of $|\psi_{ES}\rangle$ given that they only have access to the information in ρ_S ; because of this, we call our manifolds surfaces of ignorance. For an observer who only knows the information in ρ_S , the ECG gives justification for the postulate of equal a priori probabilities. We argue, as is argued in [20] and [30], that the ensemble of ρ_S in the space of purifications should be a maximally mixed distribution on the elements of F^{ρ_S} . This should be the case because, as stated by Jaynes [31], “to use any other [distribution] would amount to an arbitrary assumption of information which by hypothesis we do not have”. It should be noted that since the information in ρ_S is determined by its entanglement to ρ_E , the notion of ignorance is independent of observer and is instead an objective statement about the correlations between system and environment. The argument that entanglement is the basis for understanding the difference between subjective and objective ignorance is also given in [22].

The paper is structured as follows. In Sec. II, we give explicit expressions for the macro-states of the ECG and construct the metric and volume of the surfaces of ignorance. In Sec. III, we provide evidence that the ECG satisfies the aforementioned two key features of the BCG using examples where the symmetries of \mathcal{H}_S are given by $SO(3)$, $SU(2)$, and $SO(N)$. In Sec. IV, we generalize the ECG to include unitary transformations in \mathcal{H}_S . Finally, we conclude in Sec. V with a summary of our results and the unique traits of the ECG.

II. ENTANGLEMENT COARSE-GRAINING

In this section, we define the ECG and the associated surfaces of ignorance. We begin with a general overview of the properties of CGs. We then give explicit formulae for our macro- and micro-states. After that, we construct the metric components and compute volume of the surfaces of ignorance. Finally, we discuss the physical interpretation of the ECG in terms of thermalization and missing information of ρ_S .

A. What Makes a Coarse-Graining?

The fundamental nature of CGs is the relation between higher resolution models of a system to lower resolution models due to a lack of information in the latter. In our case, as well as in [30] and [32], reduced density operators are lower resolution models of the composite system.

To construct a CG, one must identify a set of macro-states (lower resolution data) that give relevant partial knowledge about the true state of the system. For any given macro-state, there exist many micro-states (higher resolution data) that could be responsible for it. Therefore, for a CG to be well defined, there must be a clear notion of equivalence between micro-states. That is, a

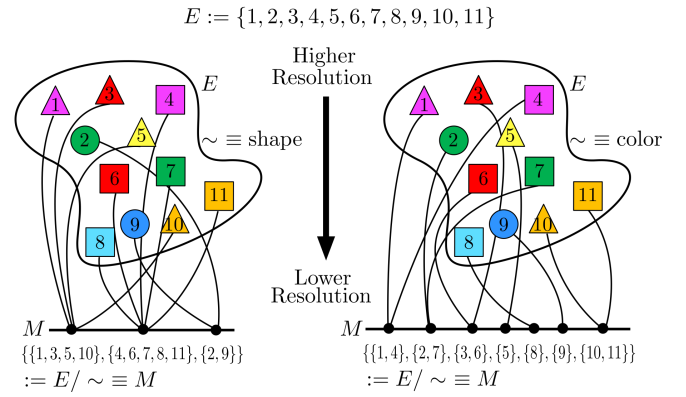


FIG. 2. Illustration of coarse-graining in terms of equivalence relations and equivalent classes. Different equivalence relations give different equivalent classes and thus different coarse-grainings. In the left figure, the equivalence relation, \sim , is shape, while on the right it is color. In both cases, we move from a higher resolution space that contains information about shape and color to a lower resolution space where information about color or shape is lost.

CG is determined by an equivalence relation that divides higher resolution data into disjoint sets called equivalent classes. Each element of an equivalence class is a micro-state, and each equivalence class is a macro-state. The equivalence relations function as constraint data (shared information) that all micro-states of a macro-state must share, and this shared information is the symmetry between micro-states. The general relationship between macro- and micro-states is summarized in Fig. 2.

The description of CGs given above is very generic. This means that any process of going from higher-resolution models to lower-resolution models by defining consistent equivalence classes constitutes a valid CG. Because of this, there are many ways to define CGs for classical and quantum systems. This is demonstrated in the literature where many quantum CGs are defined [26, 27, 30, 32–40]. In each case, the interest of the authors determines how they define their CG and why. Often, the motivation is to simplify the description of a system to make tractable problems such as tracking dynamics or performing processes like tomography. As we have stated, the ECG is motivated by defining a Boltzmann-like quantum CG for the entanglement entropy of closed many-body systems.

B. Micro- and Macro-States

In the ECG, macro-states are density operators ρ_S , and micro-states are elements of the set of purifications $F^{\rho_S} \equiv \{|\bar{\Gamma}_{ES}^{\rho_S}(\vec{\xi})\rangle\}$ such that

$$\rho_S = \text{Tr}_E \left[|\bar{\Gamma}_{ES}^{\rho_S}(\vec{\xi})\rangle \langle \bar{\Gamma}_{ES}^{\rho_S}(\vec{\xi})| \right]. \quad (1)$$

The space of the environment, \mathcal{H}_E , is taken as a copy of \mathcal{H}_S since it is sufficient to generate all purifications of ρ_S , and $\vec{\xi}$ parameterizes the transformations $U_E(\vec{\xi})$ that represent the Lie group symmetry of \mathcal{H}_E ; they are also the symmetries between micro-states.

Writing ρ_S in its spectral form

$$\rho_S = \sum_{i=1}^N \lambda^i |\lambda_S^i\rangle \langle \lambda_S^i|, \quad (2)$$

where N is the dimension of \mathcal{H}_S , the macro-data are the eigenvalues $\vec{\lambda}$. For an orthonormal basis $\{|\lambda_S^i\rangle\}$ of \mathcal{H}_S , the set of all eigenvalues that satisfy the constraint

$$\sum_{i=1}^N \lambda^i = 1, \quad (3)$$

gives a probability simplex \mathcal{S} where each element of \mathcal{S} is a valid density operator. The probability simplex is a subspace of the projective space $\mathcal{P}(\mathcal{H}_S)$, the latter of which is defined by all normalized rank 1 projectors of \mathcal{H}_S that are well defined up to $U(1)$ symmetries. Since each ρ_S on \mathcal{S} has a unique F^{ρ_S} , there exists a unique ECG of \mathcal{H}_{ES} associated with \mathcal{S} ; this is depicted in Fig. 3.

To generate F^{ρ_S} we follow the prescription given in section 5 of Wilde's "Quantum Information Theory" [41]. We begin with the canonical purification

$$|\phi_{ES}^{\rho_S}\rangle = (\hat{1}_E \otimes \sqrt{\rho_S}) |\Gamma_{ES}\rangle \quad (4)$$

in \mathcal{H}_{ES} where $\hat{1}_E$ is the identity operator in \mathcal{H}_E ,

$$|\Gamma_{ES}\rangle = \sum_{i=1}^N |\lambda_E^i\rangle |\lambda_S^i\rangle \quad (5)$$

is the unnormalized Bell state, and $\{|\lambda_E^i\rangle\}$ is a copy of $\{|\lambda_S^i\rangle\}$ in \mathcal{H}_E . From here, one can access all purifications by applying unitary transformations associated with the symmetries of \mathcal{H}_E to Eq. 4. This gives,

$$|\bar{\Gamma}_{ES}^{\rho_S}(\vec{\xi})\rangle = (U_E(\vec{\xi}) \otimes \hat{1}_S) |\phi_{ES}^{\rho_S}\rangle = (U_E(\vec{\xi}) \otimes \sqrt{\rho_S}) |\Gamma_{ES}\rangle. \quad (6)$$

In general, \mathcal{H}_E need not be a copy of \mathcal{H}_S since ρ_S can be derived from any bipartition of an arbitrary many-body system $|\psi_{ES}\rangle$. Therefore, to generalize the macro-states of the ECG given by Eq. 6 to an arbitrary purification space $\mathcal{H}_{\bar{E}S}$ where $\mathcal{H}_{\bar{E}} \neq \mathcal{H}_S$, we use the fact that all purifications of ρ_S are unitarily related.

Given the restriction that $\dim(\bar{E}) \geq N$, the ECG of \mathcal{H}_{ES} can be extended to $\mathcal{H}_{\bar{E}S}$ by

$$|\bar{\Gamma}_{\bar{E}S}^{\rho_S}(\vec{\xi})\rangle = (U_{E \rightarrow \bar{E}} \otimes \hat{1}_S) |\bar{\Gamma}_{ES}^{\rho_S}(\vec{\xi})\rangle \quad (7)$$

where

$$U_{E \rightarrow \bar{E}} = \sum_{i=1}^N |\lambda_{\bar{E}}^i\rangle \langle \lambda_E^i| \quad (8)$$

and $\{|\lambda_{\bar{E}}^i\rangle\}$ is a complete orthonormal basis of $\mathcal{H}_{\bar{E}}$. Since all macro-states of \mathcal{H}_{ES} can be extended to macro-states of some larger $\mathcal{H}_{\bar{E}S}$, we only need to consider the former to define a general ECG.

C. Surfaces of Ignorance: Metric Components and Volume

To compute the metric components and volume associated with F^{ρ_S} , we construct its first fundamental form using a Taylor expansion of Eq. 6. Expanding around parameters $\vec{\xi}_0$ using $\vec{\xi}$, the displacement vector is given by $d\vec{\xi} = \vec{\xi} - \vec{\xi}_0$. Taking the Taylor expansion of $|\bar{\Gamma}_{ES}^{\rho_S}(\vec{\xi})\rangle$ to first order, and bringing the zeroth order term to the l.h.s, the differential is given by

$$|d\bar{\Gamma}\rangle \equiv |\bar{\Gamma}(\vec{\xi}_0 + d\vec{\xi})\rangle - |\bar{\Gamma}(\vec{\xi}_0)\rangle = \sum_{i=1}^n |\bar{\Gamma}_{,\xi_i}\rangle d\xi_i \quad (9)$$

where n is the number of parameters of the symmetry. For the remainder of the paper, superscript ρ_S and subscript ES will be dropped from $|\bar{\Gamma}_{ES}^{\rho_S}(\vec{\xi})\rangle$ for simplicity of notation. Since we are working in \mathcal{H}_{ES} , and all of our states are pure, the scalar product is well defined. The metric components g_{ij} induced by the scalar product are given by the first fundamental form

$$ds^2 = \langle d\bar{\Gamma} | d\bar{\Gamma} \rangle = \sum_{i,j=1}^n \langle \bar{\Gamma}_{,\xi_i} | \bar{\Gamma}_{,\xi_j} \rangle d\xi_i d\xi_j \quad (10)$$

where $g_{ij} = \langle \bar{\Gamma}_{,\xi_i} | \bar{\Gamma}_{,\xi_j} \rangle$. From Eq. 10, the volume element is $dV = \sqrt{\text{Det}[\mathbf{g}]} d\xi_1 d\xi_2 \dots d\xi_n$ and the volume is

$$V = \int_{\xi_1} \int_{\xi_2} \dots \int_{\xi_n} dV. \quad (11)$$

Next we discuss the physical interpretation of the ECG in terms of thermalization and missing information.

D. Physical Interpretation

1. Thermalization

For a closed system $|\psi_{ES}\rangle$ whose evolution is given by

$$|\psi_{ES}(t)\rangle = U_{ES}(t) |\psi_{ES}(t_0)\rangle, \quad (12)$$

the von Neumann entropy is a constant value of zero for all t . This implies that no information is lost during the evolution and thus the process is reversible. Despite this, it is clear that the system can evolve from more ordered states where ρ_S and ρ_E are more separable to less ordered states where they are more entangled. As the system and environment interact, ρ_S has an evolution given by

$$\rho_S(t) = \text{Tr}_E \left[U_{ES}(t) |\psi_{ES}(t_0)\rangle \langle \psi_{ES}(t_0)| U_{ES}^\dagger(t) \right]. \quad (13)$$

This interaction results in an exchange of information between ρ_S and ρ_E that causes the von Neumann entropy of ρ_S to increase which indicates a greater entanglement between system and environment.

Just like the BCG, the ECG provides well defined sets of macro-states that $|\psi_{ES}\rangle$ evolves between during an information thermalization process. Here, a thermalization process is one where ρ_S goes from higher purity to lower purity due to interaction with the environment. This is illustrated in Fig. 3. We give explicit examples of the ECG in Sec. III where we show that it satisfies the two key features of the BCG discussed in the Introduction.

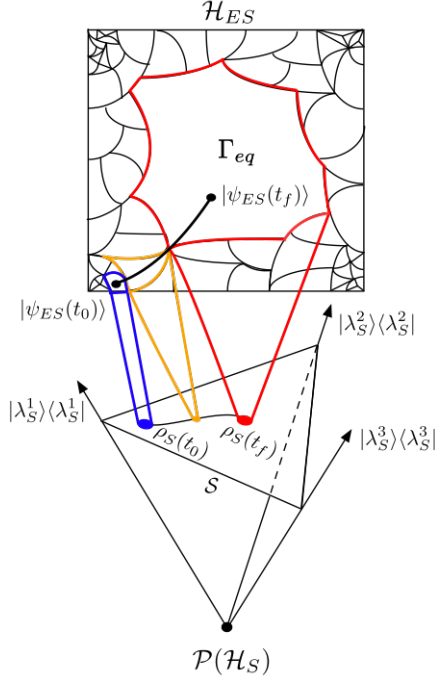


FIG. 3. A conceptual example of a thermalization process between ρ_S and ρ_E . From the perspective of ρ_S , $|\psi_{ES}\rangle$ evolves from macro-states F^{ρ_S} with smaller volume to F^{ρ_S} with larger volume. If an observer only has access to the information in ρ_S , they can't resolve the actual state of $|\psi_{ES}\rangle$ beyond the surfaces of ignorance depicted by the blue, orange, and red macro-states. This is due to the principle of a priori equal probabilities. For a global observer with access to $|\psi_{ES}\rangle$, the thermalization process is a continuous curve of pure states from $|\psi_{ES}(t_0)\rangle$ to $|\psi_{ES}(t_f)\rangle$. This is the black curve in \mathcal{H}_{ES} . Each $\rho_S \in \mathcal{S} \subset \mathcal{P}(\mathcal{H}_S)$ has one unique $F^{\rho_S} \subset \mathcal{H}_{ES}$. This implies a unique coarse-graining of \mathcal{S} in \mathcal{H}_{ES} .

2. Missing Information

An alternative interpretation of the surfaces of ignorance is that they capture the missing information in ρ_S . By missing information we mean specifically that pure states have full information and anything other than a pure state is missing information. This means that if Bob's knowledge about the state, $|\psi\rangle$, that Alice sends him is pure, then Bob is certain that the statistics of that state are represented by $|\psi\rangle$ and the expectation values $P(a^i)$ of any observable A with eigenbases $\{|a^i\rangle\}$ are

$P(a^i) = |\langle a^i | \psi \rangle|^2$. Stated another way, for a pure state $|\psi\rangle$ with zero von Neumann entropy, there exists a measurement, $|\psi\rangle\langle\psi|$ for which one is certain they will measure $|\psi\rangle$. This certainty implies full information. This is in contrast to mixed states where no such measurement exists and one is not certain which state is responsible for the statistics of the system they are measuring. Thus, there is missing information or ignorance about the state.

The relationship between the mixedness of a state and the amount of information that is missing can be understood in terms of the negentropy [42, 43]

$$I = S_{VN}^{max} - S_{VN}(\rho_S) \quad (14)$$

where $S_{VN}^{max} = \log N$, N is the dimension of \mathcal{H}_S , and $S_{VN}(\rho_S) \in [0, \log N]$ is the von Neumann entropy of ρ_S . From here we see that $I = \log N$ when $S_{VN}(\rho_S) = 0$, and $I = 0$ when $S_{VN}(\rho_S) = \log N$. This complementarity relation functions as a measure of the amount of information in ρ_S . It was shown by Brillouin [44, 45] that the negentropy of a thermodynamic system increases as the number of micro-states that are consistent with what is known about the system decreases. That is, as one gains more information, the multiplicity/volume associated with the entropy/uncertainty of the system decreases.

For the ECG, the lack of information in ρ_S manifests itself as a greater volume of F^{ρ_S} where each point on F^{ρ_S} is a purification of greater dimension that could complete the missing information in ρ_S . If one discovered which purification was responsible for ρ_S , then, according to the negentropy, they would go from having initial information $I^0 = \log N - S_{VN}(\rho_S)$ to $I^1 = \log d_{ES}$ where d_{ES} is the dimension of \mathcal{H}_{ES} . This implies an information gain of

$$\Delta I = I^1 - I^0 = \log d_{ES} - (\log N - S_{VN}(\rho)). \quad (15)$$

This gain in information is not possible without additional observations. In the absence of new information that provides a probability distribution of the likelihood that any purification is the true micro-state, a uniform (maximally mixed) distribution of all possible purifications should be assumed. This gives justification to the postulate of equal a priori probabilities, because again, as stated by Jaynes, "to use any other [distribution] would amount to arbitrary assumption of information which by hypothesis we do not have".

Given a maximally mixed distribution on F^{ρ_S} , one is less certain about which purification completes the missing information in ρ_S as the volume of F^{ρ_S} increases and is thus more ignorant about the true state of ρ_S as a subsystem of the composite system. But, one has the freedom to choose any purification to model the statistics of the subsystem since they are all consistent with ρ_S . This freedom to choose a purification may be related to a gauge freedom where the symmetry group associated with the gauge is the Lie group that captures the symmetries of \mathcal{H}_S .

Like Brillouin, the missing information in ρ_S as measured by $S_{VN}(\rho_S)$ can be measured by the number of

micro-states that are consistent with the system. In this case, the micro-states that are consistent with ρ_S are the purifications which are elements of F^{ρ_S} . Since the negentropy is simply a function of the von Neumann entropy, the relationship between negentropy and the volumes of F^{ρ_S} can be substantiated by showing the volume of F^{ρ_S} behaves like $S_{VN}(\rho_S)$ in that it is zero on pure states, maximal on maximally mixed states, and a concave function w.r.t the purity of ρ_S . That is, the volume of F^{ρ_S} can be understood as a measure of the amount of information in ρ_S via negentropy by showing that the ECG satisfies the first key feature of the BCG. This will be demonstrated for the examples considered in Sec. III.

III. VOLUME EXAMPLES

In this section, we give explicit examples of the volume associated with density operators $\rho_S \in \mathcal{S} \subset \mathcal{P}(\mathcal{H}_S)$. These examples include systems where the symmetries of \mathcal{H}_S are described by $SO(3)$, $SU(2)$, and $SO(N)$. For the $SO(3)$ and $SU(2)$ examples, we show that the resulting CGs of \mathcal{H}_{ES} are consistent with the first key feature of the BCG which is the relationship between volume, order, and equilibrium. This is demonstrated by showing that the volume and von Neumann entropy of ρ_S are both zero on pure states, maximal on maximally mixed states, and are concave functions w.r.t purity. In both cases, the volume is an upper bound of the von Neumann entropy. From this relationship between volume and S_{VN} , each surface of ignorance has a unique entanglement entropy associated with it thus connecting the ECG to the entanglement entropy.

We demonstrate that the ECG reproduces the second key feature of the BCG which is that the majority of \mathcal{H}_{ES} consists of states near or at equilibrium. We show this for low dimensions using $SU(2)$ and $SO(3)$. In these cases, the majority of \mathcal{H}_{ES} consists of states at or near equilibrium, but the trait is less pronounced because the dimension is low. Despite this, the result is clear. For $SO(3)$, we further show that the ECG satisfies the second key feature of the BCG by computing the fraction of \mathcal{H}_{ES} consisting of each macro-state. To do this, we discretize \mathcal{S} and the range of volumes of F^{ρ_S} . The additional discretization is necessary since ρ_S , F^{ρ_S} , and the volume are continuous functions of eigenvalues $\vec{\lambda}$. We also compare the volume to the linear entropy, S_L , and the von Neumann entropy and compute the average S_{VN} associated with each macro-state. From this, we see that the equilibrium macro-state is associated with high entanglement entropy.

We complete our demonstration of the second key feature by defining a general equation for the volume of $SO(N)$. The entanglement entropy of 99.99% of macro-states of \mathcal{H}_{ES} is analyzed and it is shown that the average normalized von Neumann entropy of ρ_S 's goes to one as N becomes large. This reproduces the well-known fact that the majority of states are maximally entangled.

The section is structured as follows. First we define ar-

bitrary unitary transformations for N -level systems. After that we present a detailed example of the ECG of $SO(3)$ followed by examples of $SU(2)$ and $SO(N)$.

A. Arbitrary N-Dimensional Unitary Transformations

Following the prescription in [46], any arbitrary N -dimensional unitary transformation can be written as successive transformations of 2-dimensional subspaces. Let $E^{(i,j)}(\phi_{ij}, \psi_{ij}, \chi_{ij})$ be an arbitrary transformation about the (i, j) -plane. Its components are

$$\begin{aligned} E_{kk}^{(i,j)} &= 1 & k = 1, \dots, d & \quad k \neq i, j \\ E_{ii}^{(i,j)} &= e^{i\psi_{ij}} \cos \phi_{ij} \\ E_{ij}^{(i,j)} &= e^{i\chi_{ij}} \sin \phi_{ij} \\ E_{ji}^{(i,j)} &= -e^{-i\chi_{ij}} \sin \phi_{ij} \\ E_{jj}^{(i,j)} &= e^{-i\psi_{ij}} \cos \phi_{ij} \end{aligned} \quad (16)$$

and zero everywhere else. The superscript indices (i, j) index the 2-D plane about which the transformation is applied, and the subscripts are the nonzero matrix indices. From here, one can construct successive transformations

$$\begin{aligned} E_1 &= E^{(1,2)}(\phi_{12}, \psi_{12}, \chi_{12}) \\ E_2 &= E^{(2,3)}(\phi_{23}, \psi_{23}, 0) E^{(1,3)}(\phi_{13}, \psi_{13}, \chi_{13}) \\ &\vdots \\ &\vdots \\ E_{N-1} &= E^{(N-1,N)}(\phi_{N-1,N}, \psi_{N-1,N}, 0) \end{aligned} \quad (17)$$

$$\begin{aligned} &E^{(N-2,N)}(\phi_{N-2,N}, \psi_{N-2,N}, 0) \\ &\dots E^{(1,N)}(\phi_{1N}, \psi_{1N}, \chi_{1N}) \end{aligned} \quad (18)$$

and finally an arbitrary $U(N)$ transformation

$$U = e^{i\alpha} E_1 E_2 \dots E_{N-1}. \quad (19)$$

With the arbitrary unitaries defined, we now present our examples.

B. Example: $SO(3)$

1. Computing Volume

We begin our example of $SO(3)$ by computing the volume, Eq. 11, for an arbitrary density operator $\rho_S \in \mathcal{S}$ given by Eq. 2.

From Eq. 19, the unitaries associated with $SO(3)$ are given by choosing $N = 3$ and $\alpha = \psi_{ij} = \chi_{ij} = 0$ for all i and j . This removes all complex phases, which leaves parameters $\vec{\xi} = \{\phi_{12}, \phi_{13}, \phi_{23}\}$ where $\phi_{12}, \phi_{13}, \phi_{23} \in [0, \pi/2]$. The resulting unitaries are given by

$$U(\phi_{12}, \phi_{13}, \phi_{23}) = \begin{bmatrix} \cos \phi_{12} \cos \phi_{13} - \sin \phi_{12} \sin \phi_{13} \sin \phi_{23} & \cos \phi_{23} \sin \phi_{12} & \cos \phi_{12} \sin \phi_{13} + \cos \phi_{13} \sin \phi_{12} \sin \phi_{23} \\ -\cos \phi_{13} \sin \phi_{12} - \cos \phi_{12} \sin \phi_{13} \sin \phi_{23} & \cos \phi_{12} \cos \phi_{23} & -\sin \phi_{12} \sin \phi_{13} + \cos \phi_{12} \cos \phi_{13} \sin \phi_{23} \\ -\cos \phi_{23} \sin \phi_{13} & -\sin \phi_{23} & \cos \phi_{13} \cos \phi_{23} \end{bmatrix}. \quad (20)$$

Since $U(\phi_{12}, \phi_{13}, \phi_{23})$ generates the symmetries of both \mathcal{H}_E and \mathcal{H}_S , we will use the sub-labels E and S to keep track of which space U is acting upon.

Working in the basis of \mathcal{S} , $\{|\lambda_S^i\rangle\}$ is given by

$$\{|\lambda_S^i\rangle\} = \left\{ \begin{bmatrix} 1 \\ 0 \\ 0 \end{bmatrix}, \begin{bmatrix} 0 \\ 1 \\ 0 \end{bmatrix}, \begin{bmatrix} 0 \\ 0 \\ 1 \end{bmatrix} \right\}. \quad (21)$$

This gives an explicit form of the unnormalized Bell state

given by Eq. 5. From here, all purifications are generated by

$$|\bar{\Gamma}(\vec{\xi})\rangle = \sum_{i=1}^3 \sqrt{\lambda^i} U_E(\vec{\xi}) |\lambda_E^i\rangle \otimes |\lambda_S^i\rangle. \quad (22)$$

Using Eq. 22, the nonzero metric components of $F^{\rho_S} \equiv \{|\bar{\Gamma}(\vec{\xi})\rangle\}$ are

$$g_{\phi_{12}\phi_{12}} = \langle \bar{\Gamma}_{\phi_{12}} | \bar{\Gamma}_{\phi_{12}} \rangle = \sin^2 \phi_{23} + \frac{1}{4} (\lambda^1 + \lambda^2 + 3(\lambda^1 + \lambda^2) \cos 2\phi_{23} + 2(\lambda^1 - \lambda^2) \cos 2\phi_{13} \sin^2 \phi_{23}) \quad (23)$$

$$g_{\phi_{13}\phi_{13}} = \langle \bar{\Gamma}_{\phi_{13}} | \bar{\Gamma}_{\phi_{13}} \rangle = \lambda^1 + \lambda^2 \quad (24)$$

$$g_{\phi_{23}\phi_{23}} = \langle \bar{\Gamma}_{\phi_{23}} | \bar{\Gamma}_{\phi_{23}} \rangle = \frac{1}{2} (2 - \lambda^1 - \lambda^2 - (\lambda^1 - \lambda^2) \cos 2\phi_{13}) \quad (25)$$

$$g_{\phi_{12}\phi_{13}} = g_{\phi_{13}\phi_{12}} = \langle \bar{\Gamma}_{\phi_{12}} | \bar{\Gamma}_{\phi_{13}} \rangle = (\lambda^1 + \lambda^2) \cos \phi_{23} \quad (26)$$

$$g_{\phi_{12}\phi_{23}} = g_{\phi_{23}\phi_{12}} = \langle \bar{\Gamma}_{\phi_{12}} | \bar{\Gamma}_{\phi_{23}} \rangle = -(\lambda^1 - \lambda^2) \cos \phi_{13} \sin \phi_{23} \sin \phi_{13} \quad (27)$$

where $g_{\phi_{13}\phi_{23}} = g_{\phi_{23}\phi_{13}} = 0$. Taking $\sqrt{\text{Det}(\mathbf{g})}$ gives

$$\frac{dV_{SO(3)}}{d\phi_{12}d\phi_{13}d\phi_{23}} = \sqrt{(\lambda^1 + \lambda^2)(\lambda^1 + \lambda^3)(\lambda^2 + \lambda^3)} \cos \phi_{23} \quad (28)$$

and integrating over $\vec{\xi}$ gives

$$V_{SO(3)} = (\pi^2/4) \sqrt{(\lambda^1 + \lambda^2)(\lambda^1 + \lambda^3)(\lambda^2 + \lambda^3)} \quad (29)$$

$$= (\pi^2/4) \sqrt{(1 - \lambda^1)(1 - \lambda^2)(\lambda^1 + \lambda^2)} \quad (30)$$

where the second equality is due to the constraint that the sum of the eigenvalues must equal one.

We compare Eq. 30 to the linear entropy $S_L = 1 - \text{Tr}[\rho_S^2]$ and the von Neumann entropy $S_{VN} = -\sum_{i=1}^N \lambda^i \log \lambda^i$ in Fig. 4. All three measures are normalized on the interval $L = [0, 1]$ and will be respectively referred to as $V_{SO(3)}^{\text{norm}}$, S_L^{norm} , and S_{VN}^{norm} . From Fig. 4, we see that $V_{SO(3)}^{\text{norm}}$ satisfies the first key feature of the BCG. All three functions are zero on pure states, maximal on maximally mixed states, and concave w.r.t purity. The volume also upper bounds S_{VN}^{norm} and as seen in Fig. 4d. The volume also upper bounds S_L^{norm} , but we do not show it for sake of clarity. Notice as well that $V_{SO(3)}^{\text{norm}}$ is flatter near the maximally mixed state and steeper near pure states. This is an indication that it also satisfies the second key feature of the BCG. This will be studied in more detail in Sec. IIIB 2, and generalized to higher dimensions in IIID.

From Fig 4, we showed that $V_{SO(3)}^{\text{norm}}$ behaves like an entanglement entropy. Therefore, we can associate a measure of entanglement to each macro-state of the ECG using the von Neumann entropy of ρ_S . This allows us to relate states in equilibrium of a thermalization process depicted in Fig. 3 to maximal volume since maximal volume is consistent with maximal entanglement between the system and environment. Next, we show that the majority of \mathcal{H}_{ES} consists of macro-states with maximal or near maximal volume.

2. Analyzing Volume

To show that the majority of \mathcal{H}_{ES} consists of macro-states with maximal or near maximal volume (which is to say at or near equilibrium), we use the fact that one can speak about $\rho_S \in \mathcal{S}$, $F^{\rho_S} \subset \mathcal{H}_{ES}$, and $V_{SO(3)}^{\text{norm}}$ synonymously since they are all uniquely determined by the eigenvalues $\vec{\lambda}$. Therefore, to compute the fraction of \mathcal{H}_{ES} associated with a specific F^{ρ_S} , it is sufficient to compute the fraction of \mathcal{S} consistent with a specific volume. Unfortunately, the spectrum of eigenvalues is continuous which means that the density operators and their associated volumes are not well defined. To resolve this problem, we discretize \mathcal{S} and the interval $L = [0, 1]$.

The probability simplex \mathcal{S} is discretized into finite ρ_l of equal area by uniformly sampling it using the trans-

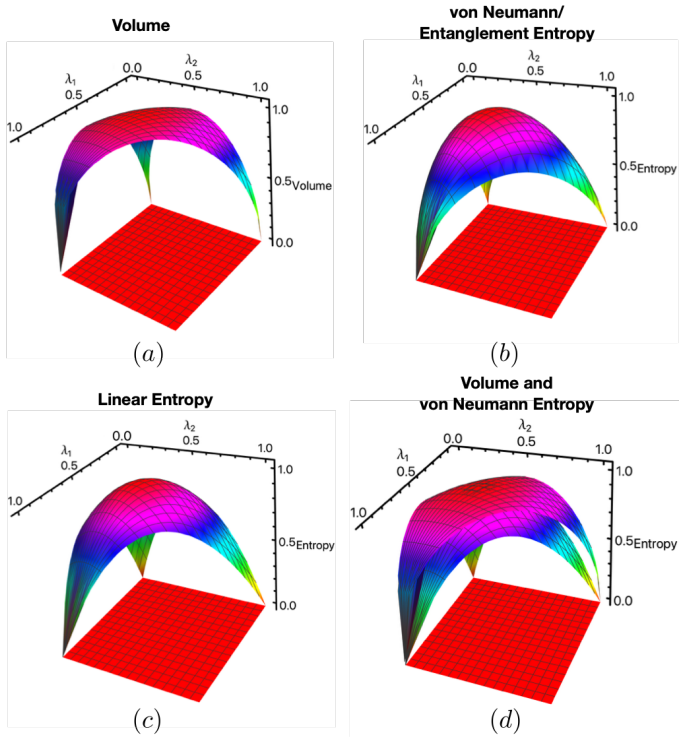


FIG. 4. Comparison between the normalizations of $V_{SO(3)}$, von Neumann entropy, and linear entropy. This demonstrates that $V_{SO(3)}$ satisfies the first key feature of the BCG which is the relationship between volume, order, and equilibrium.

formation

$$\lambda^1 = 1 - \sqrt{\eta^1} \quad (31)$$

$$\lambda^2 = \sqrt{\eta^1}(1 - \eta^2) \quad (32)$$

$$\lambda^3 = \sqrt{\eta^1}\eta^2, \quad (33)$$

where $\eta^1, \eta^2 \in [0, 1]$ are uniformly distributed in the unit interval, as seen in [47]. Dividing η^1 and η^2 into ℓ equal segments and transforming back to the $\vec{\lambda}$ basis divides \mathcal{S} into ℓ^2 discrete ρ_l , where $l \in [1, \ell^2]$; this is shown in Fig. 5b. The interval $L = [0, 1]$ is discretized by dividing it into k equal segments, L_a , where a is an integer between $[1, k]$; this is shown in Fig. 5c. Given the discretization of \mathcal{S} and L , one can compute the volume associated with each ρ_l and sort them into equivalent classes L_a . This gives the fractional volumes associated with each L_a as

$$\mathcal{V}_a = \frac{|L_a|}{|\rho_l|} \quad (34)$$

where $|L_a|$ is the number of ρ_l belonging to L_a and $|\rho_l|$ is the total number of discrete density operators.

Since $V_{SO(3)}^{\text{norm}}$, S_L^{norm} , and S_{VN}^{norm} are scalar functions on \mathcal{S} , they can be compared directly. And since they all lie on the interval L , we can compute Eq. 34 for all three using the same procedure for volume, except we replace

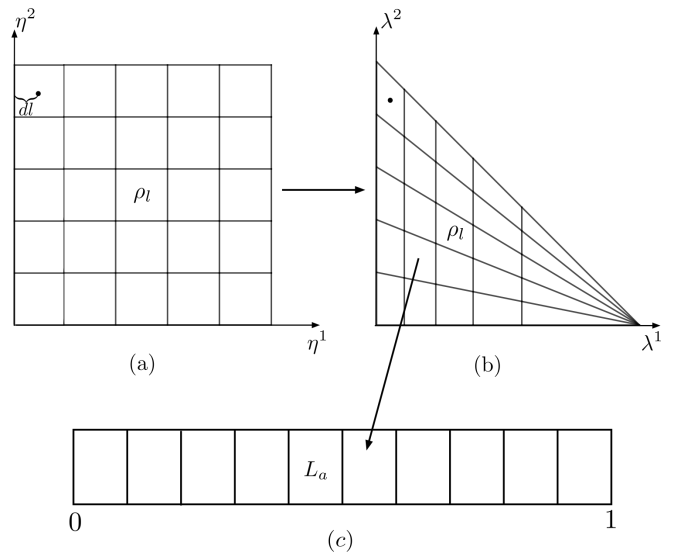


FIG. 5. Discretization of the probability simplex \mathcal{S} into discrete ρ_l of equal area, and interval $L = [0, 1]$ into segments of equal length for $\ell = 5$ and $k = 10$. In (a), we have the division of \mathcal{S} in the $\vec{\eta}$ basis while (b) is in the $\vec{\lambda}$ basis; the transformation is given by Eqs. 31 - 33. In (c), we have the sorting of ρ_l into volume equivalent classes L_a .

volume with entropies when sorting ρ_l into equivalence classes L_a .

Choosing $\ell = 300$ and $k = 10$, we compute $V_{SO(3)}^{\text{norm}}$, S_L^{norm} , and S_{VN}^{norm} at the center of squares in the $\vec{\eta}$ basis and assign that value to the corresponding ρ_l in the $\vec{\lambda}$ basis. From Fig. 5a, we see that the distance from the center of a given square is given by $dl = 1/(2\ell)$. As ℓ goes to infinity, dl goes to zero, and the volume/entropies associated with the ρ_l in the $\vec{\lambda}$ basis becomes more representative of the actual value at the center.

Coloring each ρ_l using a colormap derived from the volume and entropies assigned to them gives the first row of Fig. 6. Notice how this simply produces the contour plots of Fig. 4. To show the fraction of \mathcal{S} associated with L_a , we assign an arbitrary color to each L_a and color the ρ_l in accordance with the L_a in which they belong; this gives the second row of Fig. 6. There is nothing special about the choice of colors; they are only meant to distinguish L_a . Computing Eq. 34 and plotting the results gives the third row in Fig. 6. Due to the triangular distortions of \mathcal{S} by the transformation from $\vec{\eta}$ to $\vec{\lambda}$, these plots are produced with the restriction that $\eta^1 \in (1/4, 1]$ and $\eta^2 \in (1/2, 1]$. This guarantees the data in the analysis is within Weyl chambers [48] that do not include the triangular distortions [49] of the grid in the $\vec{\lambda}$ basis. Finally, the fourth row of Fig. 6 is the average von Neumann entropy of each L_a .

Looking at rows 3 and 4 of the first column of Fig. 6, we see that over sixty percent of \mathcal{S} consists of ρ_l belonging to L_{10} . These are states for which $V_{SO(3)}^{\text{norm}} \geq 0.9$. Further-

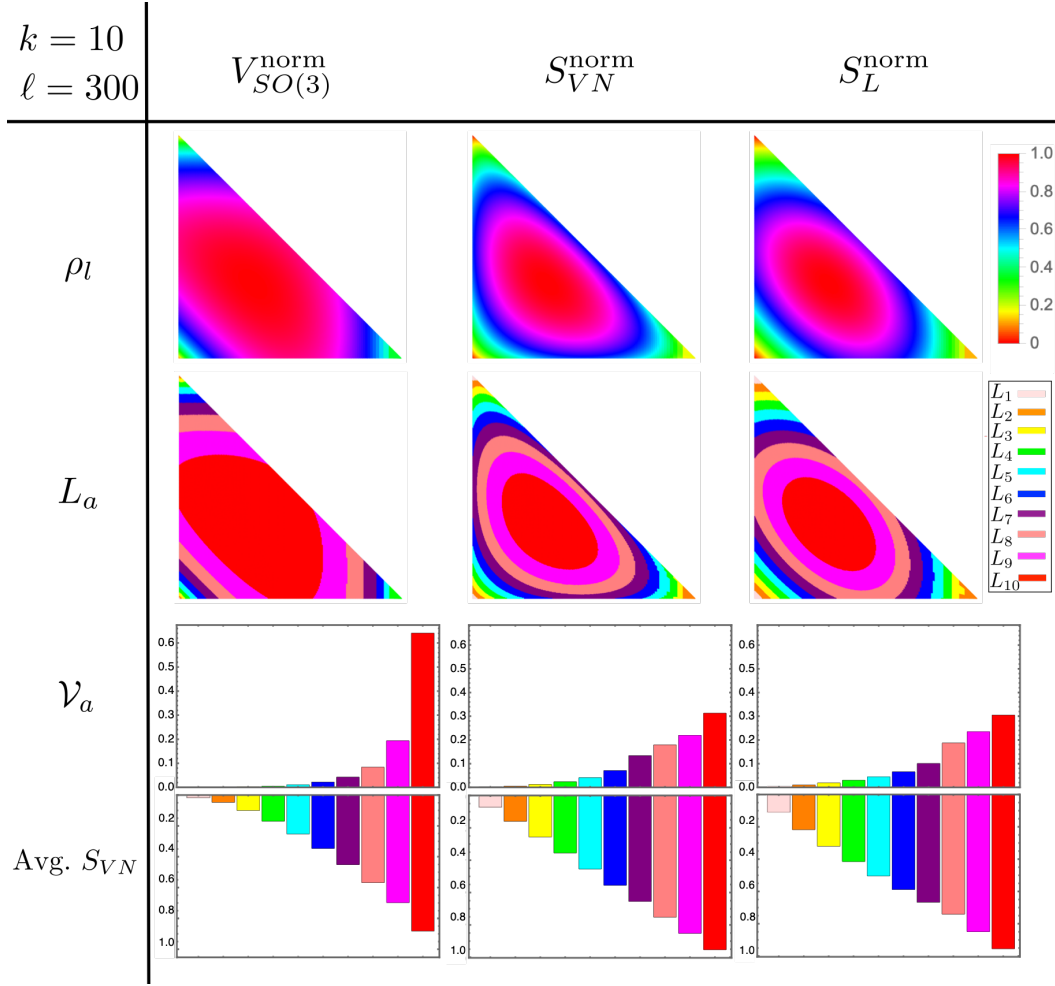


FIG. 6. Results of coarse-graining $\mathcal{H}_{ES} = \mathbb{R}^3 \otimes \mathbb{R}^3$. The first row, is the discretization of \mathcal{S} where each ρ_l is colored using the measure of each column. Row two is the result of discretizing the interval $[0, 1]$ and sorting equivalent ρ_l into segments L_a . Row three is the fraction of ρ_l belonging to each L_a . Finally, row four is the average von Neumann entropy of each L_a . It should be noted that the data from the graphs does not include the triangular distortions caused by the discretization of \mathcal{S} . We only used data from Weyl chambers that do not include triangles.

more, the average normalized von Neumann entropy of this class is 0.88 bits. This implies that the average entanglement entropy associated with L_{10} is near maximal. These results are in stark contrast to the von Neumann and linear entropies whose L_{10} volume classes make up less than thirty three percent of the total volume. This is significant because it shows that the entanglement entropy (von Neumann entropy) and linear entropy perform worse than the volumes when reproducing the second key feature of the BCG which is that most of the space of states consist of states near equilibrium. This suggests that as an entanglement measure, the volume of the surfaces of ignorance has a novel feature that is unique to the ECG procedure.

For the BCG, over 99.99% of γ -space consists of states at equilibrium. This is because it is assumed that one is working with a high dimensional system with a number of particles on the order of Avogadro's number. In this

example, we are only working with 3-level systems so the dimension of the space is vastly less. Nonetheless, we still showed that the majority of \mathcal{H}_{ES} consists of states near equilibrium. In Sec. IIID, we show that the equilibrium/maximally entangled states tend toward 99.99% as the dimension of the system goes to infinity.

C. Example: $SU(2)$

Here, we give an example for a general qubit. From Eq. 19 the unitaries of $SU(2)$ are given by

$$U(\phi, \psi, \chi) = \begin{bmatrix} e^{i\psi} \cos \phi & e^{i\chi} \sin \phi \\ -e^{-i\chi} \sin \phi & e^{-i\psi} \cos \phi \end{bmatrix} \quad (35)$$

where $\alpha = 0$, $\psi, \chi \in [0, 2\pi]$, $\phi \in [0, \pi/2]$, and the subscript 12 in the angles is dropped since the example is only 2-dimensional. Computing the metric components

directly, the nonzero values of the metric are

$$g_{\phi\phi} = \lambda^1 + \lambda^2 \quad (36)$$

$$g_{\psi\psi} = (\lambda^1 + \lambda^2) \cos^2 \phi \quad (37)$$

$$g_{\chi\chi} = (\lambda^1 + \lambda^2) \sin^2 \phi \quad (38)$$

$$g_{\phi\psi} = g_{\phi\chi} = i(\lambda^1 - \lambda^2) \cos \phi \sin \phi. \quad (39)$$

$$(40)$$

Taking the $\sqrt{\text{Det}(\mathbf{g})}$ and substituting $\lambda^2 = 1 - \lambda^1$ gives

$$dV_{SU(2)} = \sqrt{\lambda^1(1 - \lambda^1)} \sin 2\phi \, d\phi d\psi d\chi \quad (41)$$

and integrating over $\{\phi, \psi, \chi\}$ gives

$$V_{SU(2)} = 4\pi^2 \sqrt{\lambda^1(1 - \lambda^1)} = 4\pi^2 \sqrt{S_L/2} \quad (42)$$

where $\lambda^2 = 1 - \lambda^1 = \frac{1}{2} [1 + \sqrt{2 \text{Tr}[\rho^2]} - 1]$.

Like Fig. 4, we compare $V_{SU(2)}^{\text{norm}}$ with S_{VN}^{norm} and S_L^{norm} by plotting them; This is shown in Fig. 7. Again we see that all three functions are zero on pure states, maximal on maximally mixed states, and are concave function w.r.t. the purity of ρ_S . We also see again that the behavior of $V_{SU(2)}^{\text{norm}}$ deviates from S_{VN}^{norm} and S_L^{norm} in that it is flatter near maximally mixed states, steeper near pure states, and it bounds them from above. This suggests again that the ECG satisfies the first and second key features of the BCG for $SU(2)$ symmetries.

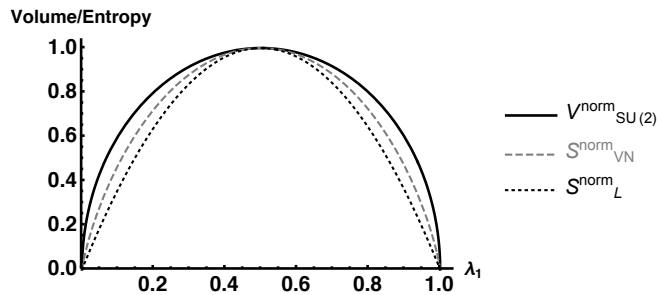


FIG. 7. Plot of the normalized volume, von Neumann, and linear entropies for 2-level systems whose symmetries are $SU(2)$.

D. Example: $SO(N)$

We complete our examples of volumes with a discussion on $SO(N)$. Computing the volume associated with $SO(2)$ by setting $\psi = \xi = 0$ in Eq. 35 gives the volume element $dV_{SO(2)} = \sqrt{\lambda^1 + \lambda^2} \, d\phi$. Inserting $dV_{SO(2)}$ into Eq. 11 and integrating ϕ from zero to $\pi/2$ gives

$$V_{SO(2)} = (\pi/2) \sqrt{\lambda^1 + \lambda^2} = \pi/2. \quad (43)$$

This result is trivial and uninteresting since $\lambda^1 + \lambda^2 = 1$, but it does provide necessary information for inferring the general form of $V_{SO(N)}$.

To generalize the volume to higher dimensions, we compute $dV_{SO(4)}$ using the same procedure from the previous examples. Unfortunately, simplifying the determinant into a usable form becomes intractable when the number of symmetry parameters is greater than three [50]. We do notice however that the volume elements $dV_{SO(3)}$, $dV_{SU(2)}$, and $dV_{SO(2)}$ are factorizable products of (radial) functions of $\vec{\lambda}$ and (angular) functions of $\vec{\xi}$, which may imply that volumes of the surfaces are product measures as seen in [48]. As such, the $\vec{\lambda}$ portion of the volume is removed from the integral, and the exact volume is merely scaled by factors of π . Assuming this form for $dV_{SO(4)}$, we set all $\vec{\xi} = 0$, since $dV_{SO(3)}$ is merely multiplied by $\cos \phi_{23}$, and get

$$\frac{dV_{SO(N)}|_{\vec{\xi}=0}}{d\xi_1 d\xi_2 \dots d\xi_{N(N-1)/2}} = \prod_{i < j}^N \sqrt{\lambda^i + \lambda^j} \quad (44)$$

where $N = 4$. To justify the choice of setting $\vec{\xi} = 0$ as valid, we numerically compute $V_{SO(4)}$ directly and compare it to Eq. 44 for $N = 4$.

Comparing the volumes given by Eq. 44 with the direct numerical integration of $dV_{SO(4)}$ where $\vec{\xi} \neq 0$ and the full integration over $\vec{\xi}$ is performed gives Fig. 8. This

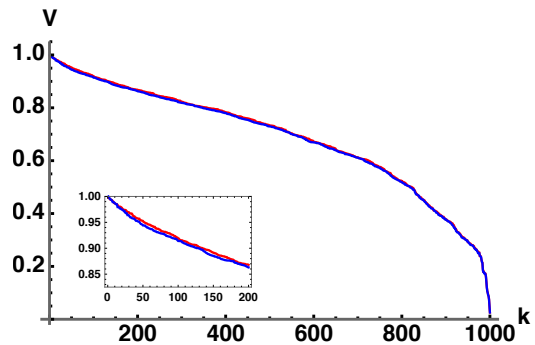


FIG. 8. Plot comparing volumes V given by Eq. 44 (red) with direct numerical integration of $dV_{SO(4)}$ (blue) vs $k \in [1, 10^3]$ density matrices that were randomly generated uniformly with respect to the Haar measure. To generate the plots, one thousand $\vec{\lambda}$'s were selected uniformly by generalizing Eqs. 31-33 to four dimensions and computing the corresponding volume. Each curve is normalized to their respective maximum volume, and (k, V) pairs are sorted by volume, in decreasing order as k increases. The red plot was computed from Eq. 44, and the blue plot is a direct integration of $dV_{SO(4)}$ using Monte Carlo integration over the $\binom{4}{2} = 10$ angles of $SO(4)$. The inset is given to show that the plots are not exactly the same, but are numerically very close.

result numerically shows that Eq. 44 (normalized to the maximum value) is a very good approximation of the actual normalized volume and that they may be in fact the same. This is not a proof, but it is a strong indication that the assumption leading to Eq. 44 is valid. We also computed $dV_{SO(5)}$, set all $\vec{\xi} = 0$ and got Eq. 44 with $N = 5$. Using these results, along with direct calculations of

$V_{SO(2)}$ and $V_{SO(3)}$, we infer by induction that the volume, barring factors of π , is

$$V_{SO(N)} = \prod_{i < j}^N \sqrt{\lambda^i + \lambda^j}. \quad (45)$$

Next, using this equation as the volume for arbitrary dimension, we show that the percentage of \mathcal{H}_{ES} consisting of states with high S_{VN} , and thus at or close to equilibrium, increases as N becomes large. The factors of π that do not appear in Eq. 45 are irrelevant to our higher dimensional analysis since it is conducted with the volume normalized.

In order to show high-entropy states comprise most of the volume of \mathcal{H}_{ES} , we consider the set of marginal density matrices

$$\rho(\lambda^1) = \lambda^1 |\lambda^1\rangle\langle\lambda^1| + \frac{1 - \lambda^1}{N - 1} \sum_{i=2}^N |\lambda^i\rangle\langle\lambda^i| \quad (46)$$

that are mixtures of a pure state and the maximally mixed state (of dimension $N - 1$) whose mixedness is parametrized by its first eigenvalue λ^1 . Inserting this choice of eigenvalues and normalizing w.r.t the maximum volume gives

$$V_{SO(N)}^{\text{norm}} = \frac{\left(\lambda^1 + \frac{1 - \lambda^1}{N - 1}\right)^{\frac{N-1}{2}} \left(2 \frac{1 - \lambda^1}{N - 1}\right)^{\frac{(N-1)(N-2)}{4}}}{\left(\frac{2}{N}\right)^{\frac{N(N-1)}{4}}}. \quad (47)$$

To show that the majority of \mathcal{H}_{ES} increasingly tends toward maximally entangled states, we plot Eq. 47 for $N = 3, 5, 7, 11$, and 30 in Fig. 9. We see that the centroid

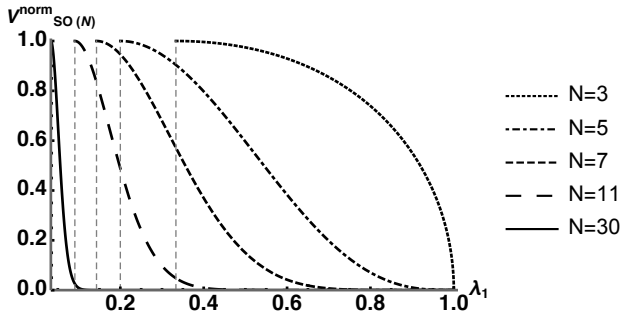


FIG. 9. Plot of $V_{SO(N)}^{\text{norm}}$ for $N = 3, 5, 7, 11, 30$. The dashed vertical lines are located at the minimal value of λ^1 for each plot, which is $1/N$, the maximally mixed state. Notice how the centroids tend toward maximally mixed states as pure states subsume less volume as N increases.

of each plot tends toward maximally entangled states as N increases. To quantify these results, we identify the value λ^{1*} for various values of N where $V_{SO(N)}^{\text{norm}}(\lambda^{1*}) = 10^{-4}$ (as a representative value [2, 8–10]). For the values of N used, this choice of λ^{1*} guarantees that

$$\frac{\int_{1/N}^{\lambda^{1*}} V_{SO(N)}^{\text{norm}}(\lambda^1) d\lambda^1}{\int_{1/N}^1 V_{SO(N)}^{\text{norm}}(\lambda^1) d\lambda^1} > 0.9999, \quad (48)$$

where $\lambda^1 = 1/N$ indicates the maximally mixed state. Plotting the average normalized von Neumann entropy between $\lambda^1 \in [1/N, \lambda^{1*}]$ as a function of N gives Fig. 10. This clearly shows that the majority of \mathcal{H}_{ES} volume tends toward maximally entangled states with increasing N .

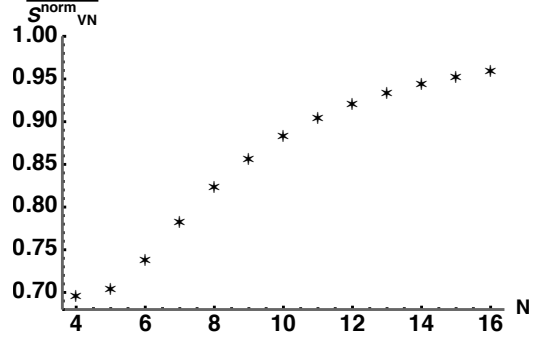


FIG. 10. Plot of the average von Neumann entropy (normalized to the maximally mixed state) between $\lambda^1 \in [1/N, \lambda^{1*}]$ as a function of N . This quantifies the results of Fig. 9 by showing that the average von Neumann entropy of states whose volumes take over 99.99% of \mathcal{H}_{ES} increases.

This analysis indicates that the ECG reproduces the second key feature of the BCG for $SO(N)$ symmetries. This also reproduces the well-known result that most states of composite systems of high dimensions are entangled [28] as the dimension increases. We did not include an analysis of $SU(N)$ since computing the determinant of the metric becomes prohibitively difficult as the number of symmetry parameters increases [50].

IV. GENERALIZING THE ENTANGLEMENT COARSE-GRAINING

In this section we generalize our formalism to include unitary transformation of \mathcal{S} in $\mathcal{P}(\mathcal{H}_S)$. This will give full freedom to define micro-states with choices of $\{\vec{\lambda}, U_E, U_S\}$.

Given an orthonormal basis $\{ |(\lambda_S^\rho)^i\rangle \}$ of \mathcal{H}_S , all unitarily related orthonormal bases can be generated by

$$\{ |(\lambda_S^\sigma)^i\rangle \} = \{ U_S |(\lambda_S^\rho)^i\rangle \}. \quad (49)$$

This gives the set of all unitarily related probability simplices \mathcal{S}^ρ and \mathcal{S}^σ in $\mathcal{P}(\mathcal{H}_S)$ depicted in Fig. 11. From here, the set of purifications associated with a density operator

$$\sigma = \sum_{i=1}^N (\lambda^\sigma)^i |(\lambda_S^\sigma)^i\rangle\langle(\lambda_S^\sigma)^i| \quad (50)$$

are given by (compare to Eq. 6)

$$|\bar{\Gamma}^\sigma(\vec{\xi})\rangle = (U_E(\vec{\xi}) \otimes \sqrt{\sigma}) |\Gamma_{ES}^\sigma\rangle \quad (51)$$

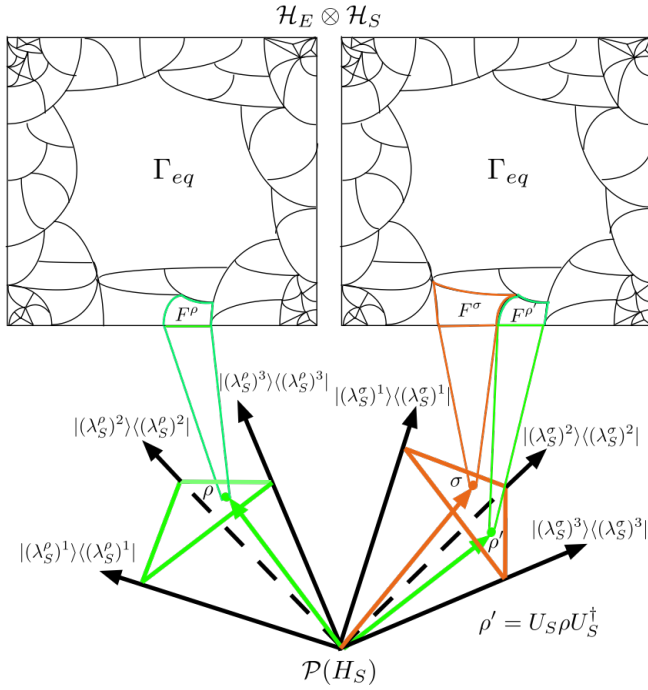


FIG. 11. Depiction of generalized entanglement coarse-graining procedure to allow unitary transformations of \mathcal{S} in $\mathcal{P}(\mathcal{H}_S)$. The green simplex on the left associated with ρ is \mathcal{S}^ρ and the orange simplex on the right associated with σ is \mathcal{S}^σ . The orthonormal basis of \mathcal{S}^σ is generated from unitary transformations U_S applied to the orthonormal basis of \mathcal{S}^ρ . Each simplex has a coarse-graining of \mathcal{H}_{ES} associated with them which are identical.

where (compare to Eq. 5)

$$|\Gamma_{ES}^\sigma\rangle = \sum_{i=1}^N |(\lambda_E^\sigma)^i\rangle |(\lambda_S^\sigma)^i\rangle. \quad (52)$$

Like Eq. 5, $\{ |(\lambda_E^\sigma)^i\rangle \}$ is a copy of $\{ |(\lambda_S^\sigma)^i\rangle \}$ in \mathcal{H}_E . Now one simply inserts Eq. 51 into Eq. 10 to get the metric components of the surfaces of ignorance associated with \mathcal{S}^σ .

This generalization may give new insights into quantum fidelity. The standard fidelity measure between arbitrary quantum states is the Uhlmann-Josza fidelity [51]. It has many equivalent definitions two of which are given by

$$\mathcal{F}_{UJ} := \max_{\{U_S\}} \text{Tr}[U_S \sqrt{\rho} \sqrt{\sigma}] \quad (53)$$

$$= \max_{\{\vec{\xi}_\rho, \vec{\xi}_\sigma\}} |\langle \bar{\Gamma}^\rho(\vec{\xi}_\rho) | \bar{\Gamma}^\sigma(\vec{\xi}_\sigma) \rangle|^2. \quad (54)$$

If ρ and σ share the same eigenbasis, Eq. 53 reduces to the fidelity of classical probability distributions. This means that the difference between classical and quantum fidelity is the relationship between unitarily related eigenbases. Additionally, Eq. 54 shows that the Uhlmann-Josza fidelity can also be understood as an optimization

over the surfaces of ignorance. Therefore, the generalized ECG may provide new geometric insights into quantum fidelity as it relates to thermalization, entanglement, and quantum CG. As far as we know, the ECG is the only procedure to define a metric and volume to the set of purifications associated with a particular density operator.

V. CONCLUSION

In this paper, we introduced the entanglement coarse-graining (ECG) which is an analogue of the Boltzmann coarse-graining (BCG) associated with the entanglement entropy for closed many-body systems, and provided examples using systems whose symmetries are defined by $SO(3)$, $SU(2)$, and $SO(N)$. The key features of the BCG captured by the ECG are (1) the relationship between volume, order, and equilibrium of a closed system, and (2) the fact that the majority of the state space consists of the equilibrium macro-state. These features are central to understanding the thermalization and reversibility of closed systems. As a system strictly becomes less ordered, it evolves from macro-states with less volume to those with greater volume until it reaches the macro-state with maximal volume. Once it reaches equilibrium, it stays there for a long time due to the second feature thus leaving observations unchanging with time. For the ECG, the equilibrium macro-state is also consistent with maximal entanglement. The feature that the majority, say 99.99%, of the state space consists of the equilibrium macro-state is the basis for arguments of typicality. Now we will summarize the traits that distinguish the ECG from other quantum coarse-grainings (CG).

The ECG is a quantum CG defined for the entanglement entropy; until now, there did not exist macro-states associated with it. This was demonstrated in Secs. III B and III C by showing that each macro-state for systems defined by $SO(3)$ and $SU(2)$ symmetries have a unique entanglement entropies associated with them. This is significant because it provides a very generic understanding of thermalization for closed quantum systems solely in terms of entanglement. As such, the ECG is a unique underlying structure of all composite Hilbert spaces thus making it broadly applicable. It also provides a clear definition of equilibrium in terms of maximum entanglement which gives a new interpretation of the well-known fact that most pure states of composite systems are maximally entangled (especially as the Hilbert space dimension increases) in terms of thermalization. Like [20], this implies that a thermalized universe is the most typical state and thus entanglement might be the basis for understanding the 2nd law of thermodynamics. The association with entanglement also gives meaning to the volume of the surfaces of ignorance as an entanglement entropy that measures the amount of information missing in ρ_S due to its entanglement with the environment.

The second unique trait is it reproduces arguments of typicality which are based on the second trait of the BCG

without assuming the dimension of the composite system is large, or assuming that $\dim(S) \ll \dim(E)$. As we showed in Sec. IIID, the second trait was reproduced for composite systems consisting of two qubits and became more pronounced as the dimension became large. As far as we know, such an analysis has not been performed prior to this work.

The third unique trait is that the macro-states of the ECG are differential manifolds generated from the Lie group symmetries that underly the Hilbert space in which the system is defined. This is in contrast to quantum CGs defined using the von Neumann projector formalism where macro-states are defined as orthogonal subspaces that are characterized w.r.t to projectors associated with observable quantities. It is also the only quantum CG that has metric components defined w.r.t its macro-states.

For future research, we plan to define a proper quantum Boltzmann entropy for the ECG. We also plan to extend our analysis to include $SU(3)$ symmetries and beyond. It would also be interesting to study the geometry of the surfaces of ignorance. This would include studies that perform isometric embeddings of real portions of the manifolds into \mathbb{R}^3 as well as comparisons of metrics for unitarily related probability simplicies. It would also be interesting to study quantum fidelity as optimization over the surfaces of ignorance.

ACKNOWLEDGMENTS

The authors wish to thank Christopher C. Tison and James E. Schneeloch for many useful discussions and inputs. PMA would like to acknowledge support of this work from the Air Force Office of Scientific Research (AFOSR). CC is grateful to the United States Air Force Research Laboratory (AFRL) Summer Faculty Fellowship Program for providing support for this work under grant #FA8750-20-3-1003. Any opinions, findings and conclusions or recommendations expressed in this material are those of the author(s) and do not necessarily reflect the views of Air Force Research Laboratory.

- [1] Jos Uffink, “Boltzmann’s Work in Statistical Physics,” in *The Stanford Encyclopedia of Philosophy*, edited by Edward N. Zalta (Metaphysics Research Lab, Stanford University, 2017) Spring 2017 ed.
- [2] Sheldon Goldstein, David A. Huse, Joel L. Lebowitz, and Roderich Tumulka, “Macroscopic and microscopic thermal equilibrium,” *Annalen der Physik* **529**, 1600301 (2017).
- [3] Harvey R. Brown, Wayne Myrvold, and Jos Uffink, “Boltzmann’s H-theorem, its discontent, and the birth of statistical mechanics,” *Studies in history and philosophy of science part B: studies in history and philosophy of modern physics* **40**, 174–191 (2009).
- [4] Sheldon Goldstein, *Chance in physics: Foundations and Perspectives* (Springer Berlin Heidelberg, 2001) pp. 39–54.
- [5] Sheldon Goldstein, Joel L. Lebowitz, Roderich Tumulka, and Nino Zanghi, *Statistical mechanics and scientific explanation: determinism, indeterminism and laws of nature* (World Scientific Publishing Co., 2020) p. 519.
- [6] R. D. Sorkin, “The Statistical Mechanics of Black Hole Thermodynamics,” in *Black Holes and Relativistic Stars*, edited by R.M. Wald (University of Chicago Press, 1998) Chap. 9, pp. 177–194.
- [7] In this work we show that the volumes we compute are upper bounded by the entropy and are in one-to-one correspondence with it. Thus, if a generic process increases the entropy, our volumes subsequently increase. Processes that increase entropy occur under very generic conditions. The following is adapted from arguments appearing on page 187–188 of Sorkin [6]. Consider an unspecified, generic evolution that takes an initial density matrix $\rho = \sum_i p_i |p_i\rangle\langle p_i| \rightarrow \sigma = \sum_i q_i |q_i\rangle\langle q_i|$, both written in their respective spectral representations, with eigenvalues $\vec{p} = \{p_i\}$ and $\vec{q} = \{q_i\}$. Consider the function $f(x) = -x \log x$ which is concave down (since $f''(x) = -1/x < 0$ for $x \geq 0$), which implies that $f(\sum_i \lambda_i x_i) \geq \sum_i \lambda_i f(x_i)$. Hence, the von Neumann entropy of the initial and final density matrices are given by $S(\rho) = \sum_i f(p_i)$ and $S(\sigma) = \sum_i f(q_i)$, respectively. Now as (classical) probabilities there exists a matrix $0 \leq T_{ij} \leq 1$ such that $q_i = \sum_j T_{ij} p_j = 1$. We only require two things of T . First, $1 = \sum_i q_i = \sum_j (\sum_i T_{ij}) p_j = \sum_j p_j \Rightarrow \sum_i T_{ij} = 1$. Second, the evolution should preserve the maximally mixed state. Namely, if $q_i = p_i = 1/N, \forall i$ then $1/N = \sum_i T_{ij} 1/N \Rightarrow \sum_j T_{ij} = 1$. These two properties indicate that T is a doubly stochastic matrix (“transition” probabilities) for which $\{q_i\}$ can be interpreted as a “mixing” of the $\{p_j\}$. Then a simple calculation shows that $S(\sigma) = \sum_i f(q_i) = \sum_i f(\sum_j T_{ij} p_j) \geq \sum_i T_{ij} \sum_j f(p_j) = \sum_j f(p_j) = S(\rho)$, where the inequality follows from the concavity of f , and the last equality follows from the first property of T . Thus, under a generic evolution of $\rho \rightarrow \sigma$ that can be characterized by the probabilities being related by a doubly stochastic matrix $\vec{q} = T\vec{p}$, the entropy will increase $S(\sigma) \geq S(\rho)$ (entropy cannot decrease under mixing).
- [8] Ludwig Boltzmann, *Lectures on Gas Theory* (Berkeley: University of California Press, 1964).
- [9] Oscar E. Landford, *Statistical Mechanics and Mathematical Problems, Lecture Notes in Physics vol. 2.* (Springer-Verlag, 1973) pp. 1–113.
- [10] H. Tasaki, “Typicality of thermal equilibrium and thermalization in isolated macroscopic quantum systems,” *J. Stat. Phys.* **163**, 937–997 (2016).
- [11] J.M. Deutsch, “Thermodynamic entropy of a many-body energy eigenstate,” *New J. Phys.* **12**, 075021 (2010).
- [12] Lea F. Santos, Anatoli Polkovnikov, and Marcos Rigol, “Weak and strong typicality in quantum systems,” *Phys. Rev. E* **86**, 010102(R) (2012).
- [13] J.M. Deutsch, Haibin Li, and Auditya Sharma, “Microscopic origin of thermodynamic entropy in isolated systems,” *Phys. Rev. E* **87**, 042135 (2013).
- [14] Adam M. Kaufman, Eric M. Tai, Alexander Lukin, Matthew Rispoli, Robert Schittkov, Philipp M. Preiss, and Markus Greiner, “Quantum thermalization through entanglement in an isolated many-body system,” *Science* **353**, 6301 (2016).
- [15] Seth Lloyd, *Black holes, demons and the loss of coherence: how complex system get information, and what they do with it* (Rockefeller University, 1988) Chap. 3.
- [16] J.M. Deutsch, “Quantum statistical mechanics in a closed system,” *Phys. Rev. A* **43**, 2046 (1991).
- [17] Mark Srednicki, “Chaos and quantum thermalization,” *Phys. Rev. E: Stat Phys Plasmas Fluids Relat Interdiscip Topics* **50**, 888–901 (1994).
- [18] Günter Mahler, Jochen Gemmer, and Mathias Michel, “Emergence of thermodynamic behavior within composite quantum systems,” *Physica E: Low-dimensional systems and nanostructures* **29**, 53–65 (2005).
- [19] Sheldon Goldstein, Joel L. Lebowitz, Roderich Tumulka, and Zanghi Nino, “Canonical typicality,” *Phys. Rev. Lett.* **96**, 050403 (2006).
- [20] Sandu Popescu, Anthony J. Short, and Andreas Winter, “Entanglement and the foundations of statistical mechanics,” *Nature Phys* **2**, 754–758 (2006).
- [21] Marcos Rigol, Vanja Dunjko, and Olshani Maxim, “Thermalization and its mechanism for generic isolated quantum systems,” *Nature* **452**, 854–858 (2008).
- [22] Noah Linden, Sandu Popescu, Anthony J. Short, and Andreas Winter, “Quantum mechanical evolution towards thermal equilibrium,” *Phys. Rev. E* **79**, 061103 (2009).
- [23] Peter Reimann, “Foundation of statistical mechanics under experimentally realistic conditions,” *Phys. Rev. Lett.* **101**, 190403 (2008).
- [24] Sheldon Goldstein and Roderich Tumulka, “On the approach to thermal equilibrium of macroscopic quantum systems,” *AIP Conference Proceedings* **1332**, 155 (2011).
- [25] Christian Gogolin and Jens Eisert, “Equilibration, thermalisation, and the emergence of statistical mechanics in closed quantum systems,” *Rep. Prog. Phys.* **79**, 056001 (2016).
- [26] D. Safranek, J. M. Deutsch, and A. Aguirre, “Quantum coarse-grained entropy and thermodynamics,” *Phys. Rev. A* **99**, 010101 (2019).
- [27] Dominik Safranek, J.M. Deutsch, and Anthony Aguirre, “Quantum coarse-graining entropy and thermalization in closed systems,” *Phys. Rev. A* **99**, 012103 (2019).
- [28] Patrick Hayden, Debbie W. Leung, and Andreas Winter, “Aspects of generic entanglement,” *Commun. Math. Phys.* **265**, 95–117 (2006).

- [29] John von Neumann, “Proof of the ergodic theorem and the H-theorem in quantum mechanics,” EPJ H **35**, 201 – 237 (2010).
- [30] Pedro Silva Correia, Paola Concha Obando, O. Raul Vallejos, and Fernando de Melo, “Macro-to-micro quantum mapping and the emergence of nonlinearity,” Phys. Rev. A **103**, 052210 (2021).
- [31] E. T. Jaynes, “Information theory and statistical mechanics,” Phys. Rev. **106**, 620–630 (1957).
- [32] Carlos Pineda, David Davalos, Carlos Viviescas, and Antonio Rosado, “Fuzzy measurement and coarse graining in quantum many-body systems,” Phys. Rev. A **104**, 042218 (2021).
- [33] P. Busch and R. Quadt, “Concepts of coarse graining in quantum mechanics,” Int. J. Theor. Phys. **32**, 2261 (1993).
- [34] O. Di Matteo, L. L. Sanchez-Soto, G. Leuchs, and M. Grassl, “Coarse graining the phase space of n qubits,” Phys. Rev. A **95**, 022340 (2017).
- [35] C. Duarte, G. D. Carvalho, N. K. Bernardes, and F. de Melo, “Emerging dynamics arising from coarse-grained quantum systems,” Phys. Rev. A **96**, 032113 (2017).
- [36] A. Singh and S. M. Carroll, “Quantum decimation in hilbert space: Coarse graining without structure,” Phys. Rev. A **97**, 032111 (2018).
- [37] O. Kabernik, “Quantum coarse graining, symmetries, and reducibility of dynamics,” Phys. Rev. A **97**, 052130 (2018).
- [38] P. Faist, *Quantum coarse-graining: An information-theoretic approach to thermodynamics*, Ph.D. thesis, ETH Zurich (2016).
- [39] S. Bartlett, T. Rudolph, and R. W. Spekkens, “Reference frames, superselection rules, and quantum information,” Rev. Mod. Phys. **79**, 555 (2007).
- [40] D. Safranek, A. Aguirre, and J.M. Deutsch, “Classical dynamical coarse-grained entropy and comparison with the quantum version,” Phys. Rev. E **102**, 032106 (2020).
- [41] M. Wilde, *Quantum Information Theory*, Quantum Information Theory (Cambridge University Press, 2013).
- [42] Erwin Schrödinger, *What is Life? The physical aspect of the living cell* (Cambridge University Press, 1944).
- [43] L. Brillouin, *Science and information theory*, 2nd ed. (Dover publications, 2013).
- [44] L. Brillouin, “Maxwell’s demon cannot operate: Information and entropy: I,” Journal App. Phys. **22**, 334 (1951).
- [45] Koji Maruyama, Franco Nori, and Vlatko Vedral, “Colloquium: The physics of Maxwell’s demon and information,” Rev. Mod. Phys. **81**, 1 (2009).
- [46] K. Zyczkowski and M. Kus, “Random unitary matrices,” J. Phys. A: Math. Gen. **27**, 4235 (1994).
- [47] K. Zyczkowski, P. Horodecki, A. Sanpera, and M. Lewenstein, “Volume of the set of separable states,” Phys. Rev. A **58**, 2 (1998).
- [48] I. Bengtsson and K. Zyczkowski, *Geometry of quantum states: An introduction to quantum entanglement*, 2nd ed. (Cambridge University Press, 2017).
- [49] The method for associating volume (or entropy) with a discrete density operator ρ_l is only valid when ρ_l is close to a regular polygon. Since the mapping from the $\vec{\eta}$ basis to the $\vec{\lambda}$ basis creates elongated triangles, the value of volume (or entropy) at the center is no longer representative of ρ_l . This can be seen in the second row of Fig. 6 where the corner associated with the triangles is mono-colored while the corners consisting of more regular polygons have a clear gradient in color. The errors in counting which ρ_l belong to which L_a are ameliorated when triangular ρ_l are not considered. And since \mathcal{S} is symmetric, their removal does not affect the results.
- [50] A $D \times D$ matrix g_{ij} has $D!$ terms in the expansion of its determinant $\text{Det}(\mathbf{g})$. $SU(N)$ ($SO(N)$) has dimension $D = N^2 - 1$ ($N(N - 1)/2$). Thus $SU(3)$ with $D = 8$ has $8! = 40,320$ terms in $\text{Det}(\mathbf{g})$ which we were unsuccessful in analytically simplifying in *Mathematica*. For $N = 4$ there are $15! \sim 1.3 \times 10^{12}$ terms which is simply impractical, even to numerically integrate. Turning to $SO(N)$, $SO(3)$ with $D = 3$ has $3! = 6$ terms in $\text{Det}(\mathbf{g})$, while $SO(4)$ with $D = 6$ has $6! = 720$ terms, the former of which could be easily simplified analytically, while the latter was at the practical limit of what could be numerically (Monte Carlo) integrated.
- [51] Richard Jozsa, “Fidelity for mixed quantum states,” Journal of modern optics **41**, 2315–2323 (1994).